Microstructural and mechanical characterization of welded joints on innovative high-strength steels

O. Holovenko, M.G. Ienco, E. Pastore, M.R. Pinasco, P. Matteis, G. Scavino, D. Firrao

The car-bodies are more and more frequently constructed with innovative high-strength steels, both to reduce the vehicles weight and to improve the passenger safety. The car-body parts are cold formed from steel sheets (manufactured by continuous casting, hot and cold rolling, and continuous heat treatment), and assembled by resistance spot welding or, less frequently, by laser welding. The welded joints obtained with the latter methods on two high-strength steels, with similar ultimate tensile strength, are examined here. An innovative, 18% Mn, austenitic TWIP steel, which exhibit a very good combination of strength and ductility, is compared with a widely used DP steel, which consists of ferrite and martensite obtained by intercritical heat treatment and fast cooling. The size and shape, defects, and microstructure of each welded joint are evidenced by metallographic examinations. Moreover, the tensile properties and the stress-life fatigue behavior of both as-received and welded specimens are compared. The fatigue strength exhibit a sharp reduction after the resistance spot welding, whereas laser welding has a much smaller effect.

Keywords: Steel, Fatigue, Welding, Automotive

INTRODUCTION

In recent years car-bodies are more and more frequently constructed with innovative high-strength steels, both to reduce the vehicles weight and to improve the passenger safety. The main requirements for these steels in service are high fracture strength and good energy absorption, in relation to the possibility of the automobile accidents, and good fatigue resistance, relatively to the normal use of vehicles [1].

In general, the high-strength steels, used so far, in comparison with the conventional deep-drawing steels show resistance characteristics three o four times higher but exhibit a reduced formability, evidenced by the smaller elongation in the tensile tests.

The steel sheets for automotive applications are normally manufactured by means of continuous casting, hot and cold rolling, continuous annealing (or other continuous thermal treatment) and, in some cases, anticorrosive coating. Steel sheets are then cold-formed (deep-drawn) in order to make car-body components. Eventually, the car bodies are constructed by assembling many deep-drawn components, often made of different steels, by using the Resistance Spot Welding (RSW) process, in which two or three superposed sheets are welded due to local heating caused by the Joule effect [2]. Laser welding (LW) [3], in which an high-power laser is employed to form a weld bead between two approached sheets, is used less frequently in the automotive industry.

Welding processes cause both microstructural and geometric effects, which can influence the fatigue behavior. In particular, the geometry of a weld spot causes a complex notch effect, which has a relevant negative influence on the fatigue performance of the welded component [4].

Dual-Phase (DP) steels are widely used, low-alloy steels, which exhibit a mixed microstructure of ferrite and martensite, which is obtained after heating to an intercritical temperature followed by a rapid cooling [5, 6].

TWIP steels for automotive uses are high-Mn steels with a significant percentage of carbon; they are not yet in common use (only one TWIP steel car-body component is known to the authors), but offer an excellent combination of strength and toughness, that is due to their austenitic structure which is strengthened by carbon and by the possibility to deform via mechanical twinning (TWIP: TWinning Induced Plasticity) [7-12].

This work is a part of a larger research project, whose goals are: to characterize and compare mass-produced, innovative, and experimental high-strength steels for car weight reduction; to facilitate the industrialization of the new steels still in the experimental stage, with regards to both the production processes and the service requirements; and

O. Holovenko, M.G. Ienco, E. Pastore, M.R. Pinasco
Dipartimento di Chimica e Chimica Industriale, Università di Genova

P. Matteis, G. Scavino, D. Firrao
Dipartimento di Scienza Applicata e Tecnologia, Politecnico di Torino

	C	Mn	Al	Ni	Cr	Si	Cu	Nb	V	P	S
DP	0,18	2,3	0,034	0,015	0,51	0,18	0,01	0,025	0,002	0,007	<0,001
TWIP	0,65	18,3	1,5	0,41	0,023	0,05	0,045	n. m.	0,04	0,025	0,011

Tab. 1 – Chemical composition of the examined steels (weight percent, n. m.: not measured).

Tab. 1 – Composizione chimica degli acciai esaminati (percentuali in peso; n. m.: non misurato).

to study the fatigue behavior of the same steels [13].
The first results obtained in this project, which are presented here, concern the microstructure and the fatigue behavior of a DP steel and of a TWIP steel, both with Ultimate Tensile Strength (UTS) close to 1 GPa, before and after welding processes performed with the aforementioned RSW and LW techniques.

MATERIALS AND METHODS

The DP steel sheets, with thickness 1.8 mm, were received after continuous annealing and zinc coating, whereas the uncoated TWIP steel sheets, with thickness 1.4 mm, were received after continuous annealing. Thereby, both steels were in the condition suitable for the industrial cold forming operations.
The chemical composition of the steels is shown in Tab. 1 and was determined by means of optical emission spectroscopy, with the exception of the Mn, Cr, Ni, Al and Cu fractions of the TWIP steel, which were determined by means of optical absorption spectroscopy after acid dissolution.
Couples of sheets of the same steel were welded by an industrial RSW apparatus, with electrode radius 3 mm and with the following process parameters: clamping force 4 kN, electric current 10 kA and duration 260 ms for the DP steel; and 3.5 kN, 7 kA and 260 ms for the TWIP steel.
Furthermore, simulated LW lines were performed on TWIP steel sheets, using a NdYAG laser with rated power 3 kW and with the following process parameters: feed rate from 2.2 to 2.7 m/min, power input from 2.4 to 2.8 kW.
Axial or transverse weld sections were mounted and mechanically polished with standard metallographic procedures. The DP steel was etched with 1% Nital (99 ml ethanol, 1 ml HCl), whereas the TWIP steel was etched with a solution of aqua regia and glycerin (1 ml HNO3, 2 ml HCl, 2 ml glycerin). The samples were then examined by optical and electron microscopy, EDS microanalyses and series of Vickers microhardness tests.
Full thickness, unnotched tensile test samples, with a calibrated region 20 mm wide and 110 mm long (Fig. 1a), were cut from the steels sheets. These samples were used at room temperature to perform both quasi-static tensile tests and stress-life fatigue test. The fatigue tests were carried out following the staircase method [14] in order to determine the fatigue strength at 1 million cycles, with load ratio zero and frequency 15 Hz. The complete rupture of a sample was used as the failure criterion.
Moreover, some tensile test samples were each welded to one sheet square, with side 20 mm, by means of one

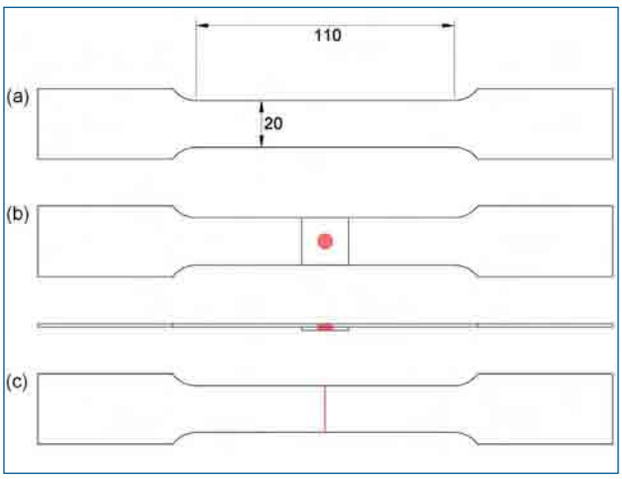

Fig. 1 - Tensile specimen (a), tensile specimen with one RSW welding spot (b) and tensile specimen with a simulated LW welding line (c), used for both the quasi-static tensile tests and the stress-life fatigue tests. Dimensions in mm and welded joints in red color.

Fig. 1 - Provino di trazione (a), provino di trazione con un punto di saldatura RSW (b) e provino di trazione con una linea di saldatura simulata LW (c), usati per le prove di trazione quasi-statiche e per le prove di durata a fatica in tensione pulsante. Quote in mm e saldature in colore rosso.

RSW spot performed in the center-point of the calibrated region (Fig. 1b). This welding process was carried out with the aforementioned RSW apparatus and process parameters, for each steel grade. Finally, another series of tensile test samples, with the same shape and size, were cut from one TWIP steel sheet, on which a simulated LW line had been previously performed with the aforementioned LW apparatus and process parameters and using helium as a protective gas; these samples were cut in such a way, that the welded line is perpendicular to the specimen tensile axis, is located at the specimen half-length, and extends over the whole specimen width (Fig. 1c).
The welded tensile test samples were then tested with the same test procedures employed for the as-fabricated sheet samples. The stress and strain applied to the welded specimens were always calculated on the basis of the samples original size, neglecting both the cross-section variations and the notch effects caused by the welded joints; for these reason, they are here defined “apparent” stress and strain.

MICROSTRUCTURE AND MICROHARDNESS

Steel sheets

The metallographic examination of the as-received steel sheets yielded the following results.
The microstructure of the DP steel (Fig. 2a) is very fine, discernible only by SEM at high magnifications, and consists of martensite and ferrite, with small fractions of bainite and retained austenite. The hardness is 290 HV 0.3 (mean of 10 tests).
The TWIP steel consists of fine grained austenite, with evi-

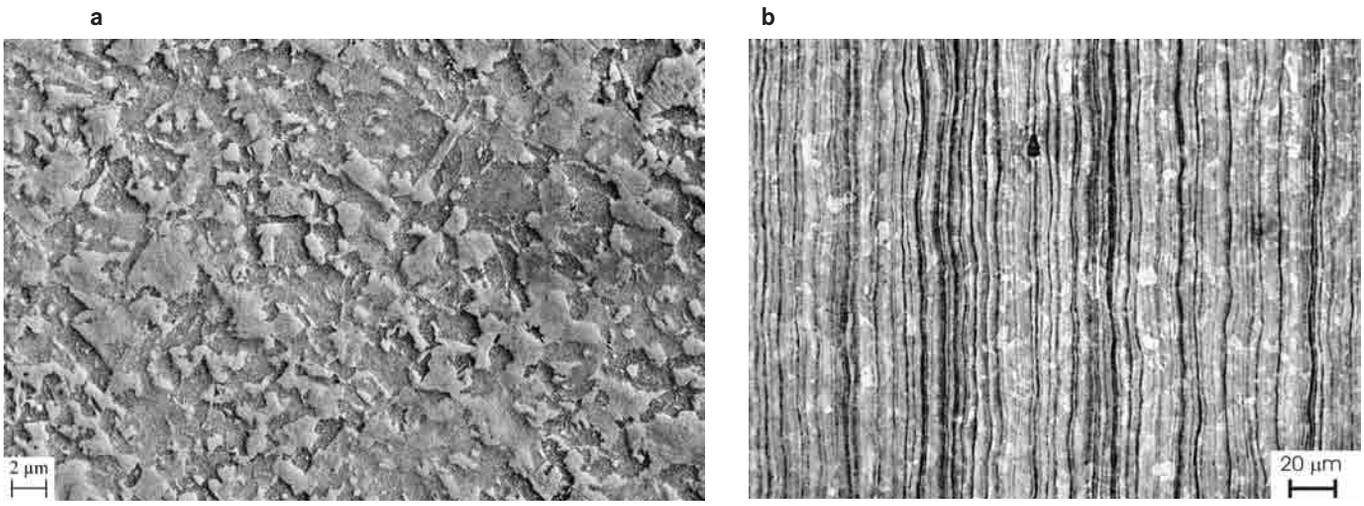

Fig. 2 - Microstructure of the examined DP (a) and TWIP (b) steels, in the as-received condition. Electron (a) and light (b) microscope.

Fig. 2 - Microstruttura degli acciai esaminati DP (a) e TWIP (b), nella condizione di fornitura. Microscopio elettronico (a) ed ottico (b

Fig. 3 - RSW welding spot between DP steel sheets. Axial metallographic section. Light microscope.

Fig. 3 - Punto di saldatura RSW tra lamiere di acciaio DP. Sezione metallografica assiale. Microscopio ottico.

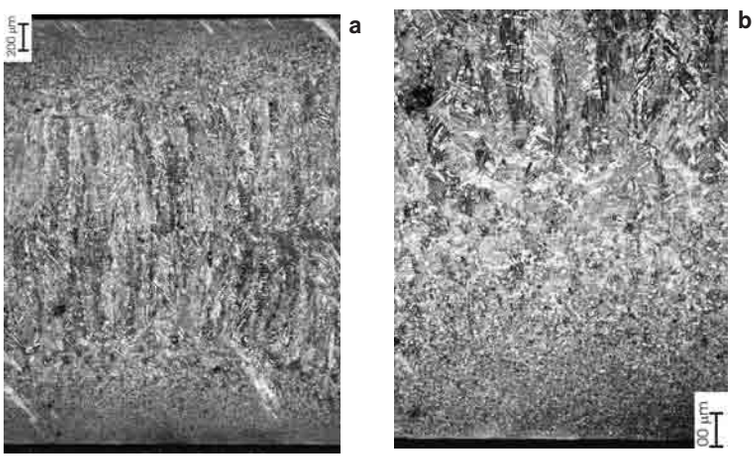

Fig. 4 - RSW welding spot between DP steel sheets. Details of Fig. 3: fusion zone and HAZ in contact with the welding electrodes; increasing magnification (a,b). Light microscope.

Fig. 4 - Punto di saldatura RSW tra lamiere di acciaio DP. Dettagli di Fig. 3: zona fusa e ZTA a contatto con gli elettrodi di saldatura; ingrandimenti crescenti (a,b). Microscopio ottico.

dent bands in the rolling directions (Fig. 2b). The hardness is 235 HV 0.3 (mean of 10 tests).

RSW joints between DP steel sheets

The metallographic examination of an axial section of an RSW joint between two DP steel sheets yielded the following results.

The shape and size of the weld region, in the examined axial section, is shown in Fig. 3. There are no evident welding defects. The fusion zone exhibit an almost regular, although not completely symmetric, elliptical shape, and does span throughout almost all the thickness of the two sheets, except the unmelted outer layers, which are about 100 µm thick. The same fusion zone exhibit a columnar dendritic structure (Fig. 4a). The dendrites grew perpendicularly from the outer edge of the weld and joined each other on the ellipse focuses and on the weld midline. In Fig. 4b the edge of the fusion zone and the Heat Affected Zone (HAZ) are visible, in the vicinity of a surface that was in contact with the welding electrode.

With the electron microscope, it can be seen that the microstructure of the molten zone consists mostly of martensite, lower bainite and retained austenite (Fig. 5a). In the HAZ, which is about 0.7 mm wide, finer and finer microstructural constituents are observed while moving away from the fusion zone, as well as ferrite traces, consistently with the pointwise temperature reached during welding (Fig. 5b). Close to the base material, the HAZ shows a microstructure similar to the base material but with larger microstructural components (Fig. 5c).

The microhardness profile (mean of 3 tests series) along a line parallel to the sheets plane and close to the weld centre is shown in Fig. 6. The fusion zone is overall uniform and much harder than the base material (on average 430 HV0.3 against 300 HV0.3), as expected for its predominantly martensitic-bainitic microstructure. In the heat affected zone, the hardness values decrease from those of the fusion zone to those of the base material, consistently with the different relative amounts and size of the microstructural constituents.

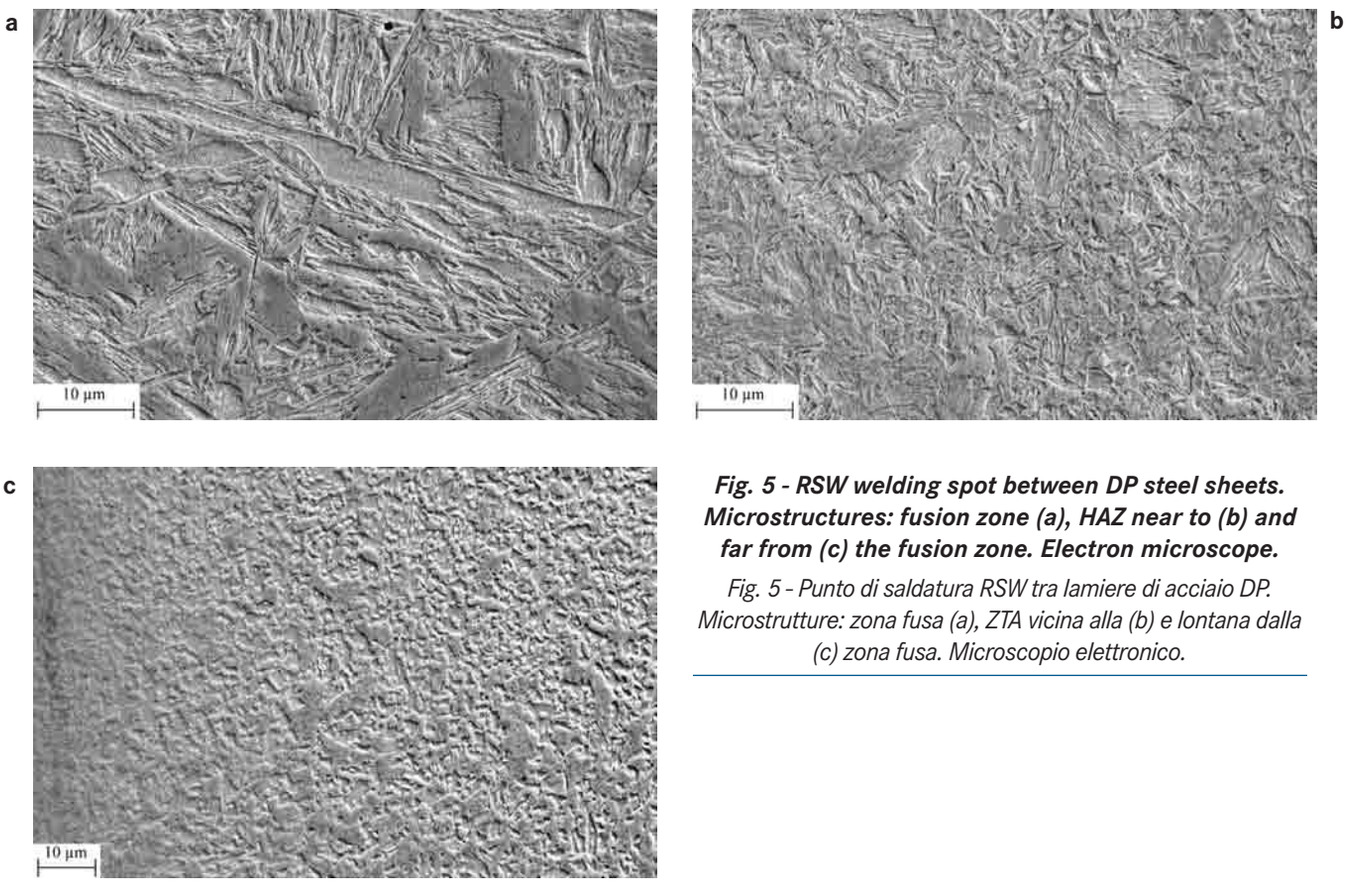

Fig. 5 - RSW welding spot between DP steel sheets. Microstructures: fusion zone (a), HAZ near to (b) and far from (c) the fusion zone. Electron microscope.

Fig. 5 - Punto di saldatura RSW tra lamiere di acciaio DP. Microstrutture: zona fusa (a), ZTA vicina alla (b) e lontana dalla (c) zona fusa. Microscopio elettronico.

RSW joints between TWIP steel sheets

The metallographic examination of an axial section of an RSW joint between two TWIP steel sheets yielded the following results.

In the examined section, Fig. 7, both the welded zone and the adjacent sheets regions, not involved in the welding process, are evident. The fusion zone is of almost regular, although not completely symmetric, elliptical shape, and it extends to almost the whole thickness of one sheet, leaving an unmelted layer about 40 µm thick on the opposite side.

At low magnification (Fig. 8a) a defective area (number 1 in the figure), a crack (2) and a porosity close to the surface (3) are already evident. At higher magnification it can be seen that the defective area is caused by large shrinkage cavities. The crack, of considerable extension (3), connects various shrinkage cavities and has a ramified appearance (Fig. 8b). Groups of interdendritic shrinkage cavities (4) are also detected by SEM and are mainly located in the centre of the fusion zone (Fig. 8c).

The microstructure of the joint consists of austenite only and has different morphology depending on the zone of the joint. The molten zone is large (the major axis is 7.7 mm) and has mainly a coarse columnar dendritic structure. The dendrites grew perpendicularly from the outer edge of the weld and joined each other on the ellipse focuses (Fig. 9a) and on the weld midline (Fig. 9b). Only at the border with the HAZ, the fusion zone exhibits a cellular microstructure (Fig. 10a, b). A relevant grain coarsening occurs in the HAZ next to the fusion zone; by increasing the distance from the fusion zone, the grain size decreases, and at 70 µm distance it is much smaller, but still greater than that of the base material (Fig. 10c). The heat affected zone is about 3 mm wide.

The EDS analyses carried out on the base material and in the molten zone showed similar composition for the elements detectable with this type of analysis. The manganese weight fraction varies from 17.7 % in the molten zone to 18.2 % in the base material; the aluminum amount is constant at around 1.5% while the silicon amount is below the instrumental detection limit. To evaluate the degree of microsegregation, some concentration profiles from a dendrite axis to the inter-dendritic area were measured: a slight manganese enrichment was found in the inter-dendritic area (Fig. 11), while the aluminum concentration is almost constant.

The microhardness profile (mean of 3 tests series) along a line parallel to the sheets plane and close to the weld centre is shown in Fig. 12. In the whole microhardness profile, a maximum hardness difference of about 40 HV is observed, with the fusion zone being the least uniform region (the lower values may be due to subsurface porosities). The average hardness of the fusion zone is comparable with that of the base material.

Simulated LW lines on TWIP steel sheets

The metallographic examination of a cross-section of a simulated LW line on a TWIP steel sheet yielded the following results.

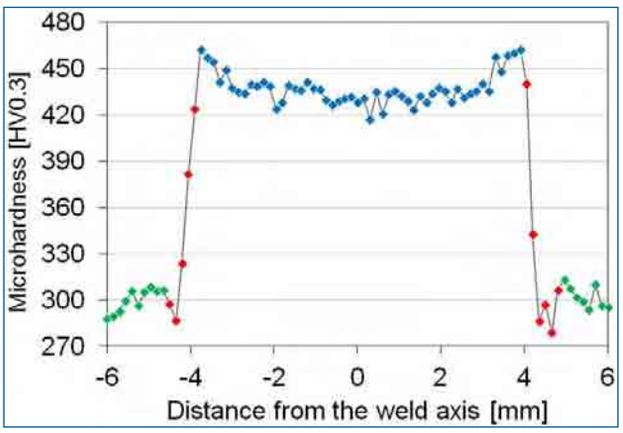

Fig. 6 - RSW welding spot between DP steel sheets. HV 0.3 Vickers microhardness along a line parallel to the sheets plane and close to the weld center (green: base metal; red: HAZ; blue: fusion zone).

Fig. 6 - Punto di saldatura RSW tra lamiere di acciaio DP. Microdurezza Vickers HV0,3 lungo una linea parallela al piano delle lamiere e vicina al centro della saldatura (verde: metallo base; rosso: ZTA; blu: zona fusa).

Fig. 7 - RSW welding spot between TWIP steel sheets. Axial metallographic section. Light microscope.

Fig. 7 - Punto di saldatura RSW tra lamiere di acciaio TWIP. Sezione metallografica assiale. Microscopio ottico.

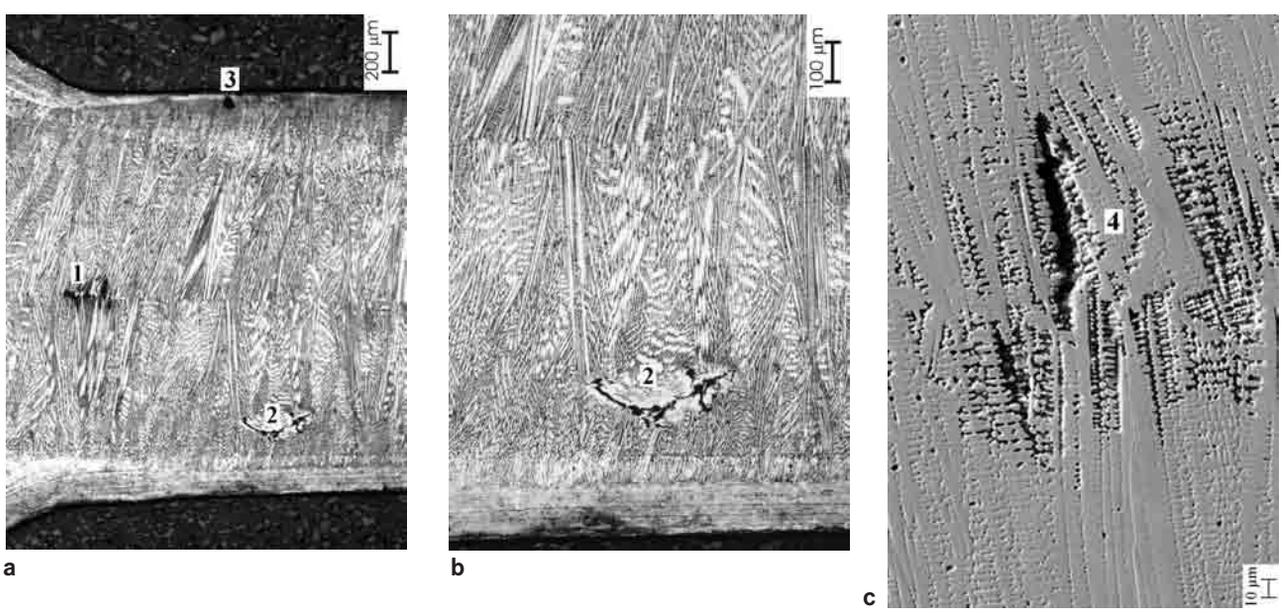

a b c

Fig. 8 - RSW welding spot between TWIP steel sheets. Details of the Fig. 7 section. Defective region (1), crack (2), porosity (3), shrinkage cavity (4). Light (a,b) and electron (c) microscope.

Fig. 8 - Punto di saldatura RSW tra lamiere di acciaio TWIP. Dettagli della sezione in Fig. 7. Zona difettosa (1), cricca (2), porosità (3), cavità di ritiro (4). Microscopio ottico (a,b) ed elettronico (c).

The whole examined cross-section of the simulated LW line is shown in Fig. 13. The crystal structure is fully austenitic both in the fusion zone and in the HAZ. The fusion zone is extended to the whole sheet thickness and its width ranges from 0.5 mm to 1.75 mm, being wider on the surface which was directly exposed to the laser beam.

The fusion zone exhibit a columnar dendritic microstructure, in which the dendrites converge with different angles on the weld symmetry plane (Figs. 13b), and micron-sized shrinkage porosities and inter-dendritic porosities, which were detected by SEM (Fig. 14b). A grain coarsening can be observed in the HAZ next the fusion zone; by increasing the distance from the fusion zone, the grain size gradually decreases and at 0.6 mm distance it is similar to that of the base material (Fig. 14a).

The microhardness profile (mean of 3 tests series) along a line perpendicular to the weld symmetry plane is shown in Fig. 15. The hardness is slightly higher in the base material and lower in the fusion zone. In the HAZ, the hardness is intermediate and decreases close the fusion zone, consi-

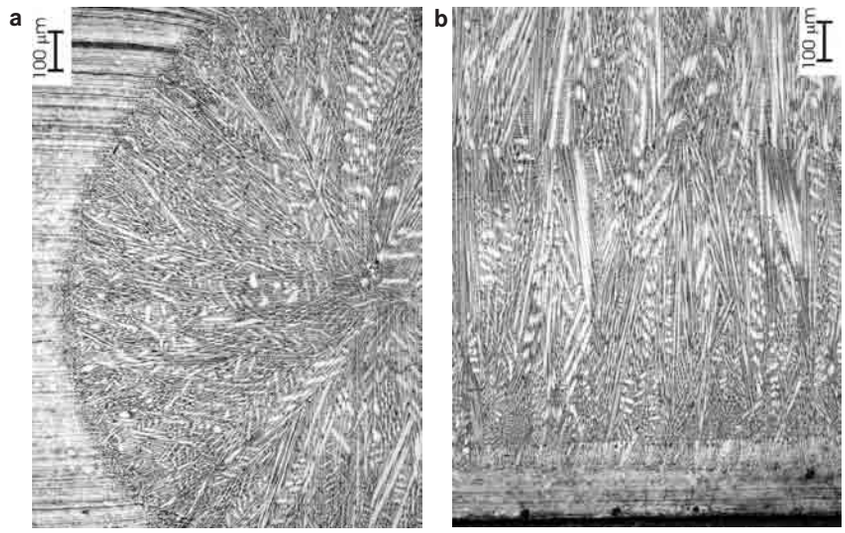

Fig. 9 - RSW welding spot between TWIP steel sheets. Details of the Fig. 7 section. Rough dendritic structure. Light microscope.

Fig. 9 - Punto di saldatura RSW tra lamiere di acciaio TWIP. Dettagli della sezione in Fig. 7. Struttura dendritica grossolana. Microscopio ottico

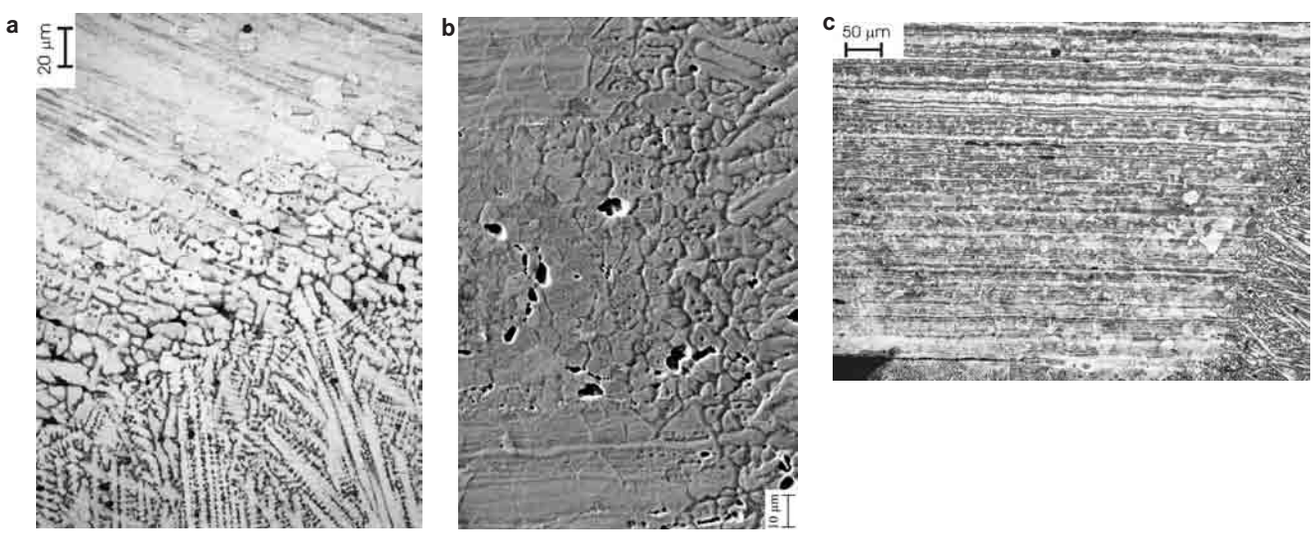

Fig. 10 - RSW welding spot between TWIP steel sheets. Boundary of the fusion zone (a,b) and HAZ (c). Light (a,c) and electron (b) microscope.

Fig. 10 - Punto di saldatura RSW tra lamiere di acciaio TWIP. Margine della zona fusa (a,b) e ZTA (c). Microscopio ottico (a,c) ed elettronico (b).

stently with the increase of the grain size. The maximum difference between the hardness values is 50 HV. Similar microhardness profiles, performed elsewhere, yield similar results, but with somewhat different widths of the fusion zone and of the HAZ.

MECHANICAL PROPERTIES

The yield stress, fracture stress and elongation at rupture of the DP steel are 705 MPa, 1013 MPa, and 13 %, whereas the same properties of the TWIP steel 488 MPa, 1007 MPa, and 47 %, respectively (Fig. 16). The two DP steel samples, welded with one RSW spot, which were tested in traction, broke far away from the weld spot itself and their apparent tensile curves are almost identical to the tensile curve of the as received DP steel.

The welded TWIP steel tensile test samples, on the contrary, were always broken close to the welded joint; their apparent tensile curves are initially almost identical to the tensile curve of the as received TWIP steel, but then exhibit an earlier rupture, with fracture stress and elongation at rupture equal to 796 MPa and 14 %, for the sample with the RSW spot, and to 868 MPa and 21 %, for the sample with the simulated laser line, respectively (Fig. 16).

The results obtained from the fatigue tensile tests are represented in Fig. 17. The fatigue strength (here defined as the maximum stress, or stress amplitude, which corresponds to a 50 % survival probability after 1 million cycles) of the DP and TWIP steels is 570 and 410 MPa, respectively.

The apparent fatigue strength of the TWIP steel samples with the simulated LW line, namely 400 MPa, is almost equal to the fatigue strength of the as received TWIP steel; this is further confirmed by the fact that two of these samples (not used to calculate the fatigue limit) were broken in fatigue away from the welded joint. The TWIP steel samples with the RSW spot, on the contrary, show considerably lower fatigue resistance, i.e. 210 MPa for the TWIP steel and 190 MPa for the DP steel, and were always

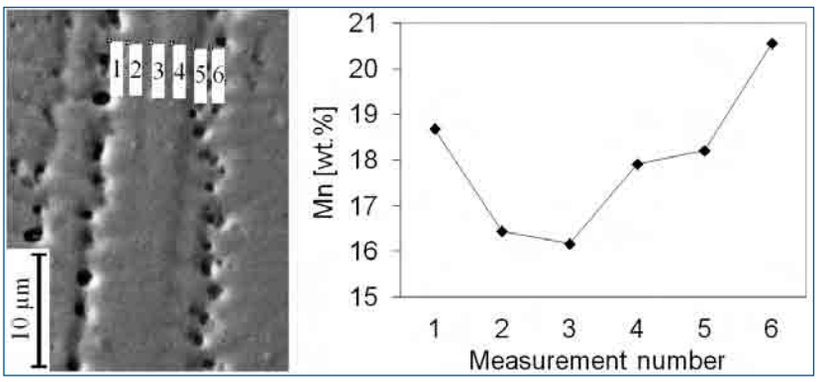

Fig. 11 - RSW welding spot between TWIP steel sheets. EDS microanalysis. Weight percent Mn from a dendrite axis to the interdendritic region.

Fig. 11. Punto di saldatura RSW tra lamiere di acciaio TWIP. Microanalisi EDS. Percentuale in peso di Mn dall'asse di una dendrite alla zona infradenditrica.

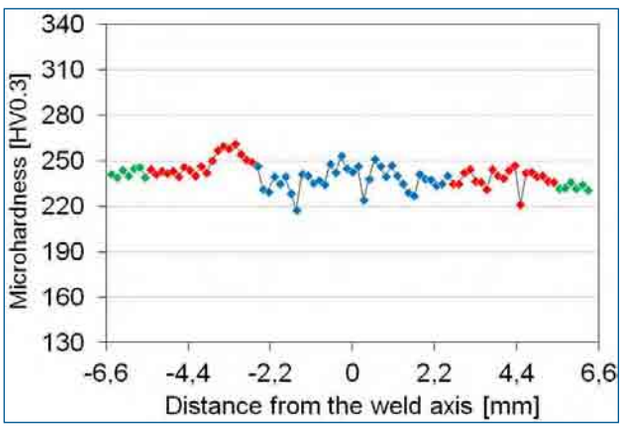

Fig. 12 - RSW welding spot between TWIP steel sheets. HV0.3 Vickers microhardness along a line parallel to the sheets plane and close to the weld center (green: base metal; red: HAZ; blue: fusion zone).

Fig. 12 - Punto di saldatura RSW tra lamiere di acciaio TWIP. Microdurezza Vickers HV0,3 lungo una linea parallela al piano delle lamiere e vicina al centro della saldatura (verde: metallo base; rosso: ZTA; blu: zona fusa).

a

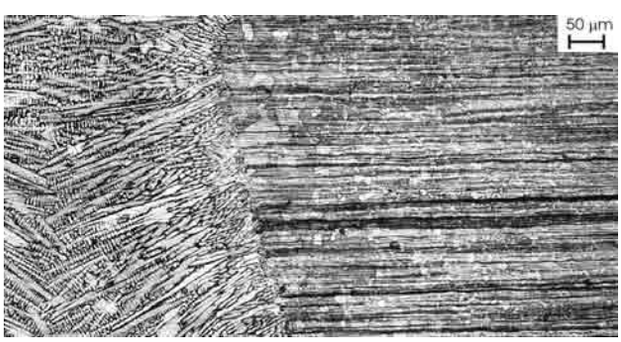

b

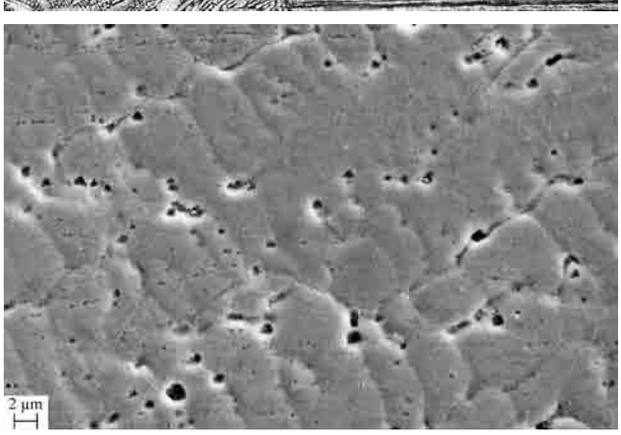

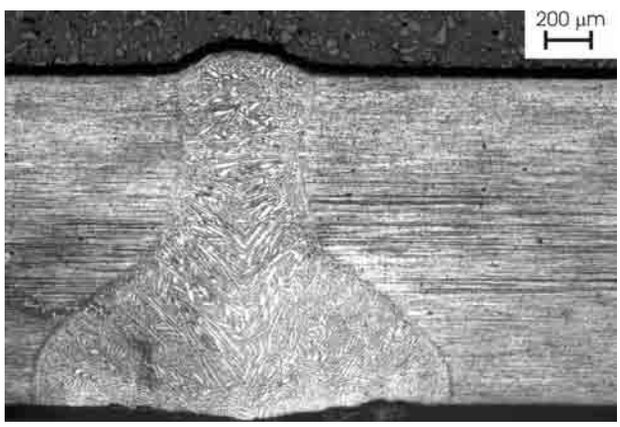

a

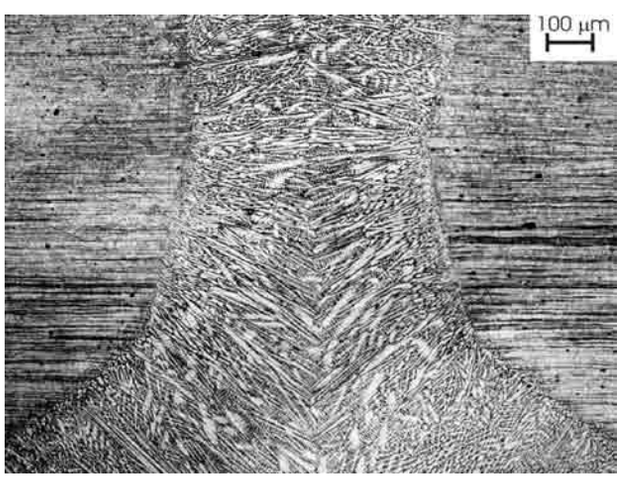

b

Fig. 13 - Simulated LW welding line in a TWIP steel sheet. Transversal metallographic section (a) and magnification (b). Light Microscope.

Fig. 13 - Linea di saldatura simulata LW in una lamiera di acciaio TWIP. Sezione metallografica trasversale (a) ed ingrandimento (b). Microscopio ottico.

Fig. 14 - Simulated LW welding line in a TWIP steel sheet. Details of Fig 13: melted zone and HAZ (a); melted zone (b). Light (a) and electron (b) microscope.

Fig. 14 - Linea di saldatura simulata LW in una lamiera di acciaio TWIP. Dettagli di Fig. 13: zona fusa e ZTA (a); zona fusa (b). Microscopio ottico (a) ed elettronico (b).

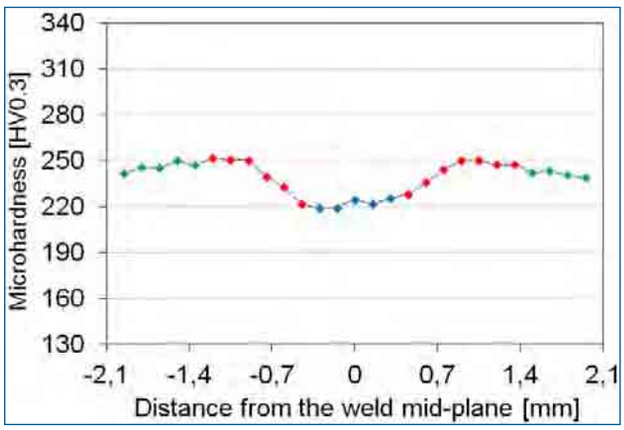

Fig. 15 - Simulated LW welding line in a TWIP steel sheet. HV0.3 Vickers microhardness along a line perpendicular to the weld symmetry plane (green: base metal; red: HAZ; blue: fusion zone).

Fig. 15 - Linea di saldatura simulata LW in una lamiera di acciaio TWIP. Microdurezza Vickers HV0,3 lungo una linea perpendicolare al piano di simmetria della saldatura (verde: metallo base; rosso: ZTA; blu: zona fusa).

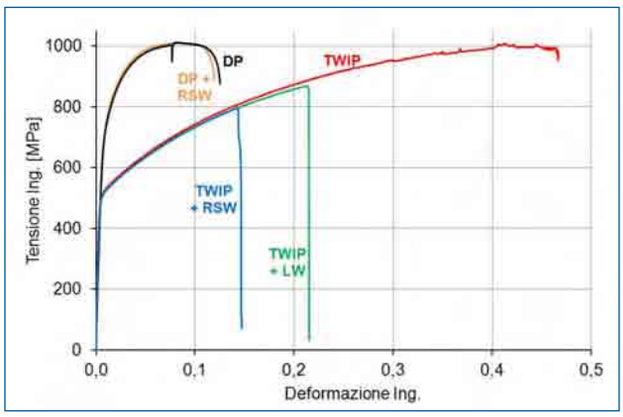

Fig. 16 - Tensile curves of the DP and TWIP steels, either as-received or welded with the RSW or LW methods.

Fig. 16 - Curve di trazione degli acciai DP e TWIP tal quali ricevuti o saldati con i metodi RSW o LW.

broken in or around the weld spots themselves.

CONCLUSIONS

The microstructure, tensile properties and fatigue behavior of two high-strength car-body steels, namely a widely used dual-phase ferritic-martensitic steel and a new high-Mn austenitic TWIP steel, were studied both in the as-fabricated state and after welding.

The resistance welding spots performed between the DP steel sheets are free of macroscopic defects. The microstructure in the fusion zone consists of martensite and bainite, whereas in the HAZ it consists of the same phases and of a small amount of ferrite. The microhardness of the fusion zone is greater than that of the base material, with an increment of 150 HV.

The resistance welding spots performed between TWIP steel sheets exhibit both macroscopic and microscopic shrinkage cavities and porosities. The simulated welding lines performed on TWIP steel sheets, on the contrary, do not show welding defects. In both cases, the microhardness is almost uniform, with differences smaller than 40 HV, and the microstructure is fully austenitic, with different morphologies in the different zones of the weld.

The ultimate tensile strength of both steels is close to 1 GPa, but the DP steel exhibit an higher fatigue strength at 1 million of cycles, i.e. 570 MPa, versus 410 MPa for the TWIP steel. This fact may be explained by considering the FCC crystal structure and the lower yield stress of the TWIP steel, which imply that the microplasticity phenomena, which promote the fatigue crack nucleation, may occur at lower stress in the TWIP steel, in comparison with the DP steel.

After homologous resistance spot welding, both DP and TWIP steels show a much lower apparent fatigue strength (at 1 million cycles). In the DP steel case, this reduction, from 570 to 190 MPa, must be attributed both to notch effect caused by the geometry of the weld spot and to the different mechanical properties of the microstructures observed in the fusion zone and in the heat affected zone. In the TWIP steel case, instead, the reduction of the apparent fatigue strength, from 410 to 210 MPa, must be attributed mainly to the notch effect, combined with the presence of welding defects, since the crystal structure and the hardness do not differ significantly throughout the fusion zone, the heat affected zone and the base material.

The latter conclusion is also consistent with the fatigue strength of the samples subjected to the simulated laser welding, which is almost equal to that of the as-received material. In fact, the TWIP steel samples, subjected to the simulated laser welding, in comparison with those subjected to the resistance spot welding, exhibit nearly identical microstructures (even if the weld size is different), but only much smaller (usually micrometric) solidification defects and no relevant notches.

The relevance of the notch effect, caused by the welding spots, implies that the results presented here, regarding the resistance spot welded specimens, are a function of the weld spot size, relative to the sample width, and they cannot be easily extrapolated to the other types of welding joints.

REFERENCES

[1] S. Maggi, G. Scavino, “Fatigue characterization of automotive steel sheets”, 11th International Conference on Fracture, Torino, Italy, 2005

[2] N.T. Williams, “Resistance spot welding”, in: D.L. Olson et al. (eds.), ASM Handbook, Vol. 6, ASM International, Materials Park, Ohio, USA, 1993, 226 - 229

[3] J. Mazumder, “Laser-beam welding”, in: D.L. Olson et al. (eds.), ASM Handbook, Vol. 6, ASM International, Materials Park, Ohio, USA, 1993, 262 - 268

[4] S. Zhang, “Stress intensities at spot welds”, International Journal of Fracture 88 (1997) 167 - 185

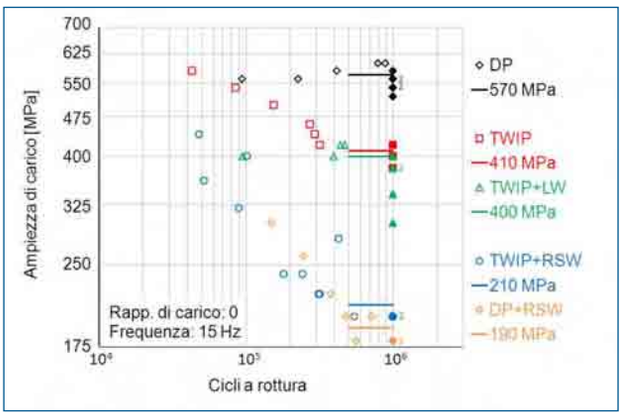

Fig. 17 - Wohler diagram of the DP and TWIP steels, either as-received or welded with the RSW or LW methods, and respective 1 million cycles fatigue strength (50% survival probability); not broken specimens are reported with filled symbols and numbers of repetitions.

Fig. 17 - Diagramma di Wohler degli acciai DP e TWIP tal quali ricevuti o saldati con i metodi RSW o LW e rispettiva resistenza a fatica ad 1 milione di cicli (probabilità di sopravvivenza 50%); i provini non rotti sono indicati con simboli pieni e numeri di ripetizioni.

[5] G.R. Speich, "Dual-phase steels", in: J.R. Davis et al. (eds.), ASM Handbook, Vol. 1, ASM International, Materials Park, Ohio, USA, 1990, 424 - 429

[6] CEN prEN 10338, "Cold rolled flat products of multiphase steels for cold forming - technical delivery conditions", CEN, Bruxelles, 2010

[7] D. Cornette, P. Cugy, A. Hildenbrand, M. Bouzekri, G. Lovato, "Ultra high strength FeMn TWIP steels for automotive safety parts", Revue de Metallurgie 102 (2005) 905 - 918

[8] L. Chen, H.S. Kim, S.K. Kim, B.C. De Cooman, "Localized deformation due to Portevin–LeChatelier effect in 18Mn–0.6C TWIP austenitic steel", ISIJ International 47 (2007) 1804 - 1812

[9] P.D. Zavattieri, V. Savic, L.G. Hector, J.R. Fekete, W. Tong, Y. Xuan, "Spatio-temporal characteristics of the Portevin–Le Chatelier effect in austenitic steel with twinning induced plasticity", International Journal of Plasticity, 25 (2009) 2298 - 2330

[10] G. Scavino, F. D'Aiuto, P. Matteis, P. Russo Spena, D. Firrao, "Plastic localization phenomena in a Mn-alloyed austenitic steel", Metallurgical and Materials Transactions A 41 (2010) 1493 – 1501

[11] O. Bouaziz, S. Allain, C. P. Scott, P. Cugy, D. Barbier, "High manganese austenitic twinning induced plasticity steels: a review of the microstructure properties relationships", Current Opinion in Solid State and Materials Science 15 (2011) 141 - 168

[12] G. Scavino, C. Di Salvo, P. Matteis, R. Sesana, D. Firrao, "Portevin–Le Chatelier effects in a high-Mn austenitic steel", Metallurgical and Materials Transactions A 44 (2013) 787-792

[13] P. Matteis, G. Scavino, F. D'Aiuto, D. Firrao, "Fatigue behavior of dual-phase and TWIP steels for lightweight automotive structures", Steel Research International 83 (2012) 950 - 956

[14] UNI 3964, "Prove meccaniche dei materiali metallici. Prove di fatica a temperatura ambiente. Principi generali", UNI, Milano, 1985

Caratterizzazione strutturale e meccanica di giunti saldati in acciai altoresistenziali innovativi

Parole chiave: Acciaio - Fatica - Saldatura - Automotive

Le scocche degli autoveicoli sono sempre più spesso costruite con acciai altoresistenziali, sia per ridurre il peso, sia per migliorare la sicurezza passiva [1]. Le parti delle scocche sono imbutite usando lamiere di acciaio e sono poi unite con saldature a punti a resistenza (RSW) [2], le quali causano rilevanti effetti di intaglio [4], oppure, più raramente, con saldature laser [3]. In questo lavoro si esaminano giunti saldati omologhi realizzati con detti metodi su due acciai altoresistenziali, di analoga resistenza a rottura. L'acciaio innovativo TWIP contenente il 18% di Mn, con microstruttura austenitica [7-12], è confrontato con un acciaio DP di uso corrente con microstruttura di ferrite e martensite [5-6].
LAMIERE ESAMINATE - Le lamiere di acciaio DP, spesse 1,8 mm, sono state esaminate dopo trattamento termico continuo e zincatura; le lamiere di acciaio TWIP, di spessore 1,4 mm, non rivestite, dopo ricottura continua. La microstruttura dell'acciaio DP come ricevuto (Fig. 2a) è molto fine ed è costituita da martensite e ferrite, con piccole frazioni di bainite e di austenite residua. La durezza media è 290 HV0,3. L'acciaio TWIP come ricevuto è costituito da austenite fine con una evidente bandizzazione (Fig. 2b). La durezza media è 235 HV0,3.
METODI SPERIMENTALI - Coppie di campioni di lamiere omologhe sono state saldate con un impianto industriale di saldatura RSW. Inoltre, sono state eseguite linee di saldatura laser simulata su fogli di lamiera di acciaio TWIP. Dalle lamiere sono stati fabbricati provini di trazione (Fig. 1a) usati sia per prove di trazione quasi-statica, sia per prove di fatica in tensione pulsante, svolte con il metodo staircase, per determinare la resistenza ad 1 milione di cicli, con

rapporto di carico zero. Una parte dei provini di trazione sono stati saldati a quadrati di lamiera omologhi (Fig. 1b). Inoltre, una ulteriore serie di campioni di trazione sono stati ricavati da un foglio di lamiera TWIP, nel quale era stata eseguita una linea di saldatura LW simulata (Fig. 1c). I provini di trazioni saldati sono stati poi provati con le medesime procedure usate per i campioni di lamiera tal quale; sia nelle prove di trazione, sia in quelle di fatica, le tensioni e le deformazioni sono state calcolate sulla base delle dimensioni originali del campione.
GIUNTI DP-DP SALDATI A PUNTI (RSW) - Si evidenzia una zona fusa di forma ellittica (Fig. 3) con struttura colonnare dendritica (Fig. 4a). La microstruttura della zona fusa è costituita da martensite, bainite inferiore ed austenite residua (Fig. 5a). Nella ZTA, ampia circa 0,7 mm, allontanandosi dalla zona fusa, si osservano elementi strutturali con dimensioni via via minori e tracce di ferrite, coerentemente con la temperatura raggiunta durante la saldatura.
Nel complesso la durezza (Fig. 6) risulta uniforme nella zona fusa, con valori più elevati rispetto al materiale base (430 HV0,3 contro 300 HV0,3); nella ZTA si osservano valori decrescenti da quelli della zona fusa a quelli del materiale base.
GIUNTI TWIP-TWIP SALDATI A PUNTI (RSW) - La zona fusa, di forma ellittica, occupa quasi tutta la sezione (Fig. 7). Si osservano una zona difettosa (numero 1 in Fig. 8a), una cricca (2) e, vicino alla superficie esterna, una porosità (3). La zona difettosa è riconducibile a grosse cavità di ritiro. La cricca (3) collega diverse cavità di ritiro ed ha aspetto ramificato (Fig 8b). La sola fase presente è austenite. La zona fusa (asse maggiore = 7,7 mm) ha struttura dendritica colonnare grossolana; solo al confine con la ZTA assume struttura tendenzialmente cellulare (Figg. 9, 10a,b). Nella ZTA (Fig. 10c) la taglia del grano è notevole al confine con la zona fusa; poi diminuisce allontanandosi e a 70 μm è sensibilmente ridotta, pur restando superiore a quella del materiale base. La zona termicamente alterata si estende per circa 3 mm. La massima differenza fra i valori di durezza (Fig. 12) è circa 40 HV.
LAMIERA TWIP CON SIMULAZIONE DI SALDATURA LASER (LW) - La zona fusa (Fig. 13) ha ampiezza variabile da 1,75 mm a 0,5 mm ed è più ampia sulla superficie illuminata dal laser. La struttura della zona fusa è a dendriti colonnari (Fig. 14a); sono presenti microcavità di ritiro e porosità interdendritiche di dimensioni micrometriche (Fig. 14b). La microstruttura è costituita dalla sola austenite. Nella ZTA si osserva ingrossamento del grano al confine con la zona fusa, con dimensioni che decrescono fino a raggiungere quelle del materiale base ad una distanza di circa 0,6 mm (Fig. 14a).
La durezza (Fig.15) è lievemente maggiore nel materiale base e minore nella zona fusa. I valori di durezza della ZTA sono intermedi e calano avvicinandosi alla zona fusa.
PROPRIETÀ MECCANICHE - La tensione di snervamento, la tensione di rottura e l'allungamento a rottura sono: 705 MPa, 1013 MPa e 13% per l'acciaio DP, 488 MPa, 1007 MPa e 47% per l'acciaio TWIP, rispettivamente. I due campioni di trazione di acciaio DP, recanti un punto di saldatura RSW, si sono rotti lontano dai punti di saldatura, con curve di trazione apparenti uguali a quella dell'acciaio tal quale (Fig. 16). I campioni di trazione saldati di acciaio TWIP, invece, si sono rotti sempre in prossimità della saldatura, con curve di trazione apparenti sovrapponibili alla parte iniziale di quella dell'acciaio tal quale, ma con rottura anticipata. La tensione di rottura e l'allungamento a frattura apparenti sono 796 MPa e 14% per la saldatura RSW, 868 MPa e 21% per la saldatura laser (Fig. 16).
La resistenza a fatica degli acciai DP e TWIP (ad 1 milione di cicli) è 570 e 410 MPa, rispettivamente (Fig. 17). I campioni di acciaio TWIP sottoposti alla saldatura laser presentano una resistenza a fatica pressoché uguale a quella dell'acciaio tal quale (400 MPa). I campioni con un punto di saldatura a resistenza hanno, invece, una resistenza a fatica molto minore, 210 MPa nel caso dell'acciaio TWIP e 190 MPa per l'acciaio DP.
CONCLUSIONI - La resistenza a rottura di entrambi gli acciai è prossima ad 1 GPa, ma l'acciaio TWIP offre una minore resistenza a fatica, che si può spiegare considerando la sua struttura CFC ed il suo minor valore di tensione di snervamento. Dopo la saldatura a punti, la resistenza a fatica apparente di entrambi gli acciai è molto ridotta. Nel caso dell'acciaio DP, tale riduzione è attribuibile in parte all'effetto di intaglio ed in parte alle diverse microstrutture osservate nella zona fusa e nella zona termicamente alterata. Nell'acciaio TWIP, invece, la medesima riduzione è attribuibile prevalentemente all'effetto di intaglio, combinato con la presenza di difetti di saldatura. Questa ultima considerazione è corroborata dalla resistenza a fatica dei campioni di acciaio TWIP sottoposti alla saldatura laser, che è pressoché uguale a quella del materiale base.